



Improving the air coupling of bulk piezoelectric transducers with wedges of power-law profiles: A numerical study



Marcel C. Remillieux^{*}, Brian E. Anderson, Pierre-Yves Le Bas, T.J. Ulrich

Geophysics Group EES-17, Los Alamos National Laboratory, MS D446, Los Alamos, NM 87545, USA

ARTICLE INFO

Article history:

Received 21 October 2013
Received in revised form 13 February 2014
Accepted 15 February 2014
Available online 4 March 2014

Keywords:

Piezoelectric transducers
Air-coupled ultrasound
Acoustic-structure interaction
Finite-element analysis
Time-reversed acoustics

ABSTRACT

An air-coupled ultrasonic transducer is created by bonding a bulk piezoelectric element onto the surface of a thick plate with a wedge of power-law profile. The wedge is used to improve the ultrasonic radiation efficiency. The power-law profile provides a smooth, impedance-matching transition for the mechanical energy to be transferred from the thick plate to the air, through the large-amplitude flexural waves observed in the thinnest region of the wedge. The performance of the proposed transducer is examined numerically and compared to that of a design where the piezoelectric element is isolated and where it is affixed to a thin plate of uniform thickness. The numerical analysis is first focused on the free-field radiation of the transducers. Then, time-reversal experiments are simulated by placing the transducers inside a cavity of arbitrary shape with some perfectly reflecting boundaries. In addition to time-reversal mirrors, the proposed concept could be integrated in the design of phased arrays and parametric arrays.

Published by Elsevier B.V.

1. Introduction

The ability to create a high-amplitude excitation focused in space and time is critical to achieve high-resolution imaging in nondestructive evaluation (NDE) of elastic structures [1,2]. Other applications include medical needs (imaging, hyperthermia, and lithotripsy) [3] and underwater communication [4]. NDE techniques rely increasingly on air-coupled transducers due to the many advantages they offer. As bonding between the transducer and the structure is no longer necessary, rapid imaging of large areas is then becoming possible.

Air-coupled transducers can be separated mainly in two categories: bulk piezoelectric transducers and micro-machined ultrasonic transducers (MUTs). The first category is still used extensively for NDE applications. A bulk piezoelectric transducer performs well when its impedance is of the same order of magnitude as that of the medium it is coupled to. For this reason, they are preferred when bonding with the test specimen is possible and high amplitude excitation is required. For the same reason, coupling with air is problematic because of the impedance mismatch, by several orders of magnitude, between air (~ 400 Rayl) and typical piezoelectric materials (~ 35 MRayl). This limitation is most commonly addressed by the use of matching layers [5,6] but at the expense of

a reduced bandwidth and the subsequent ringing of the device. The second category of air-coupled transducers (MUTs) offers excellent impedance matching with air, a broader bandwidth, and a reduction in size of the apparatus. However, these transducers cannot be fabricated and implemented without micro-fabrication capabilities. Capacitive MUTs have been introduced in the 1990s [7,8]. A single element of these transducers typically consists of an air-filled cavity enclosed on one side by a stretched, flexible, metallic membrane (sensing and emitting element) and on the opposite side by a rigid conducting back plate, which drives the membrane through an applied alternating voltage. More recently, piezoelectric MUTs have been developed by using thin piezoelectric membranes [9–11], thus removing the need for a conducting back plate. An electric field is applied across the thickness of the piezoelectric film, which in turn induces a deformation of the membrane according to its bending modes.

Ultrasonic arrays of transducers have been increasingly preferred over single-element transducers because they offer more flexibility in the type of ultrasonic fields generated, better imaging capabilities, and may be used to focus ultrasonic energy at desired locations. Drinkwater and Wilcox [12] give an extensive review on this topic, focusing on phased arrays, where the transducer materials and array geometries are discussed. The operation of phased arrays is based on the use of appropriate time delays between the signals applied to or received from the individual transducers. Although widely used, phased arrays suffer from a number of limitations. First, computing time delays in a reverberant environment

^{*} Corresponding author. Tel.: +1 5403150577.

E-mail addresses: mcr1@lanl.gov (M.C. Remillieux), bea@lanl.gov (B.E. Anderson), pylb@lanl.gov (P.-Y. Le Bas), tju@lanl.gov (T.J. Ulrich).

is not a trivial task. Second, it is important to reduce or ideally eliminate the cross-talk between the transducers so that they can be controlled independently. Third, the performance of a phased array is limited by the number of transducers.

An alternative strategy consists of using the concept of time reversal (TR) with an array of transducers to create a TR mirror (TRM) [13,14]. Unlike a phased array, this device can focus energy in space and time without *a priori* knowledge of the time delays between the transducer signals. Besides, its performance increases with the amount of scattering in the environment. In fact, the size of the TRM can be reduced to a single element in a reverberant environment of non-regular shape, which is often referred to as a *chaotic cavity* [15–18]. The multiple reflections in the environment act as virtual transducers (additional degrees of freedom) that can be used to improve the quality of the focusing. On the other hand, the non-regular shape of the environment breaks any symmetry that could potentially exist in the problem. Based on this concept, Etaix et al. [19] proposed an air-coupled TRM where a bulk piezoelectric transducer is glued onto a thin plate for 3D imaging applications (e.g. detection of objects) in air. The high modal density of the plate vibration provides the required reverberant environment in 2D. The focusing in 3D is achieved through the fluid–structure interaction. Other than shape and size, the modal density of the plate vibration can also be increased in a limited bandwidth via an array of periodically-spaced resonators (metamaterial-inspired approach) connected to the plate [20]. Le Bas et al. [21] developed an air-coupled TRM for NDE applications where relatively large amplitude of the focused energy is required to excite the non-linear features (e.g. crack, delamination, and other flaws) of the test sample. Their device consists of an acoustic cavity of pyramidal shape enclosed by thin metallic walls onto which bulk piezoelectric transducers are glued. The cavity creates a diffuse wave field inside, through the vibration of the walls, the multiple reflections inside the cavity, and the fluid–structure interaction. The cavity also contains an opening to allow a progressive emission of the scattered waves toward the location where ultrasonic energy should be focused. This work follows directly that from Arnal et al. [22] where a chaotic cavity was developed to focus ultrasonic energy in water. It is worth mentioning that it is easier to achieve higher pressure levels in water than in air because the fluid–structure coupling is more important when the structure is light relative to the surrounding fluid (i.e. better impedance matching).

In the recent work on air-coupled TRMs, little attention has been devoted to improving the impedance matching for the coupling of the piezoelectric transducers to the air. Optimizing the acoustic output of the transducers is critical to achieve a sufficient signal-to-noise ratio and to develop a useful tool for imaging or non-contact NDE applications. In this paper, the possibility of using bulk piezoelectric ceramics as efficient air-coupled transducers is examined numerically using finite-element (FE) analysis. The concept of wedges of power-law profiles and their properties on the propagation of flexural waves are exploited for this application. This concept has been used to mitigate plate vibration for automotive and aerospace applications at low frequencies (e.g. <10 kHz) [23,24] but, to the authors' knowledge, not yet to enhance the sound radiation from piezoelectric transducers or for the design of air-coupled ultrasonic arrays. This work intends to bridge the gap between the practicality of using bulk piezoelectric ceramics and the sound-radiation efficiency of MUTs.

This paper is organized as follows. Section 2 introduces the theory behind the propagation of elastic waves in a wedge of power-law profile. This section also describes the main physical mechanisms involved in the problem, including wave propagation in elastic solids, piezoelectric effect, propagation of sound in the surrounding fluid, and fluid–structure interaction. Section 3 describes the numerical model settings and analyzes the free-field

ultrasonic radiation of various ultrasonic transducers. Specific attention is given to the acoustic radiation from wedges of power-law profiles. In Section 4, the performance of the proposed design is discussed in the context of a numerical TR experiment. Section 5 concludes.

2. Problem description and resolution

The problem considered in this paper is the vibration of and sound radiation from a bulk piezoelectric element and the plate it is affixed to, as depicted in Fig. 1. Away from the interface between the plate and the piezoelectric element, the thickness of the plate is not necessarily uniform but may decrease smoothly from h_0 to h_1 over the distance x_0 as,

$$h(x) = \frac{(h_0 - h_1)(x_0 - x)^m}{x_0^m} + h_1, \quad \forall x \in [0, x_0] \quad (1)$$

where m is a positive real number.

2.1. Flexural waves in a wedge of power-law profile

Starting from thin-plate theory, it is possible to demonstrate that flexural waves propagating along a wedge of a power-law profile, such as that depicted in Fig. 1, will exhibit low propagation velocities with the elastic energy eventually concentrating near the wedge tip [25,26].

The differential equation governing the motion of a thin plate in vacuum with a variable thickness in the x -direction may be expressed as [27],

$$D(x)\nabla^4 w + 2\frac{dD(x)}{dx}\frac{\partial}{\partial x}\nabla^2 w + \frac{d^2D(x)}{dx^2}\left(\frac{\partial^2 w}{\partial x^2} + \nu\frac{\partial^2 w}{\partial y^2}\right) + \rho h(x)\frac{\partial^2 w}{\partial t^2} = 0 \quad (2)$$

where $w(x,y)$ is the normal displacement of the mid-plane of the thin plate, $h(x)$ is the local thickness of the plate, ρ is the mass per unit volume, $D(x)$ is the local flexural rigidity defined as $D(x) = Eh(x)^3/(12(1 - \nu^2))$, E is the Young's modulus, and ν is the Poisson ratio. Using geometrical acoustics, the local wavenumber of a plane flexural wave in a wedge with profile $h(x)$ may be expressed as,

$$k(x) = 12^{1/4}k_p^{1/2}h(x)^{-1/2} \quad (3)$$

where $k_p = \omega/c_p$ is the wavenumber of a symmetrical plate wave, ω is its angular frequency, and $c_p = 2c_s\sqrt{1 - (c_s/c_l)^2}$ is its phase

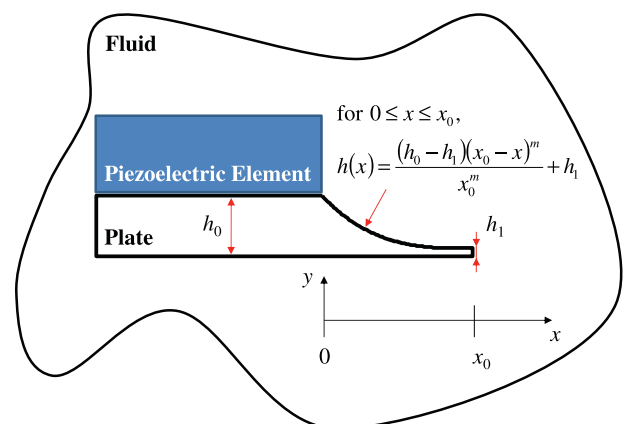


Fig. 1. Schematic representation of the system to be modeled.

velocity, with c_l and c_s the longitudinal and shear velocities in the material, respectively. Integrating Eq. (3) along the length of the wedge and using the profile $h(x)$ given in Eq. (1) provides an expression of the integrated wave phase,

$$\phi = \int_0^{x_0} \left[12^{1/4} k_p^{1/2} \left(\frac{(h_0 - h_1)(x_0 - x)^m}{x_0^m} + h_1 \right)^{-1/2} \right] dx \quad (4)$$

If the wedge has no truncation ($h_1 = 0$) and $m \geq 2$, then ϕ diverges. Physically, this means that the wave never reaches the wedge tip and never reflects back from it either. It becomes trapped near the wedge tip, which is referred to as the “acoustic black hole effect” by Krylov. A similar demonstration can be made for a wedge immersed in a fluid. In this case, $m \geq 5/3$ for the integrated wave phase to diverge. If all the vibrational energy concentrates in the thinnest region of the wedge, it is expected that acoustic radiation in the surrounding fluid will be the largest near this point. This theoretical result is used here as the basis for improving the coupling of piezoelectric transducers to the air. However, it should be kept in mind that in practice, a wedge is always truncated in some way ($h_1 > 0$). Due to this imperfection, part of the vibration energy will be reflected back from the wedge tip, which will deteriorate the sound radiation efficiency of the wedge.

2.2. Main physical mechanisms involved

The problem is formulated in the framework of linear dynamics. It is assumed that the thick plate is made of a homogeneous material and is not subject to body forces. The small-amplitude displacement, \mathbf{u} , of a material point, \mathbf{r} , from its equilibrium position can be described by the Navier equation, expressed in vector form as,

$$\mu \nabla^2 \mathbf{u} + (\lambda + \mu) \nabla (\nabla \cdot \mathbf{u}) = \rho_s \frac{\partial^2 \mathbf{u}(\mathbf{r}, t)}{\partial t^2} \quad (5)$$

where λ and μ are the Lamé constants of the material, ρ_s is the density of the material, and $\mathbf{r} = (x_1, x_2, x_3)$ are the Cartesian coordinates of a point in the solid medium.

A piezoelectric material is characterized by its ability to convert electrical energy into mechanical energy, and vice versa. The linear, electro-elastic constitutive relation for a piezoelectric material can be expressed in stress-charge form as,

$$\mathbf{T} = \mathbf{c}^E \mathbf{S} - \mathbf{e}^T \mathbf{E} \quad (6)$$

$$\mathbf{D} = \mathbf{e} \mathbf{S} + \boldsymbol{\varepsilon}^S \mathbf{E} \quad (7)$$

where \mathbf{T} is the vector of mechanical stress components, \mathbf{D} is the vector of electric displacement components, \mathbf{S} is the vector of mechanical strain components, \mathbf{E} is the vector of electric field components, \mathbf{c}^E is the elastic stiffness matrix at constant electric field, \mathbf{e} is the matrix of piezoelectric stress constants, and $\boldsymbol{\varepsilon}^S$ is the matrix of permittivity components at constant strain. The superscript T indicates that the matrix is transposed.

As the elastic components of the system vibrate, they radiate sound into the surrounding fluid medium. In the absence of internal sources of energy (e.g. monopoles and dipoles), the linear propagation of sound in a lossless medium is governed by the homogeneous wave equation,

$$\frac{1}{c^2} \frac{\partial^2 p(\mathbf{r}, t)}{\partial t^2} + \Delta p(\mathbf{r}, t) = 0 \quad (8)$$

where p is the acoustic pressure, c is the speed of sound (or acoustic wave velocity) within the medium, and $\mathbf{r} = (x_1, x_2, x_3)$ are the Cartesian coordinates of a point in the fluid medium. In this problem, the acoustic sources are modeled as boundary conditions using the fluid–structure coupling mechanism.

Fluid–structure interaction occurs at the interface between all structural elements (e.g. piezoelectric element and wedged plate) and the surrounding fluid medium (e.g. air). The interface conditions must define the fluid loading on the elastic domain as well as the effects of the structural deformation on the fluid. More specifically, coupling is enforced as follows: (i) the fluid applies a force per unit area equal to the total pressure (ambient atmospheric pressure + acoustic pressure) on the surfaces of the elastic elements and (ii) the particle acceleration of the fluid must match the normal component of the structural acceleration at the fluid–structure interface.

2.3. Numerical resolution

The above problem is solved in the time domain, using the “Acoustic-Piezoelectric Interaction” module of the commercial FE software package COMSOL MULTIPHYSICS 4.3a [28]. Models are built in two dimensions to reduce the computational cost of the numerical simulations. Each model consists of up to three subdomains, including a piezoelectric material, a linear elastic material (if any), and a fluid. The dependent variables of the problem are the displacement field (two components), the electric potential, and the pressure. The system equations are discretized with quadratic triangular elements. The maximum element size is constrained to a fifth of the smallest wavelength involved in the problem to ensure convergence of the solution. The discretized system equations are integrated in time using the generalized- α method [29], which is a fully implicit, unconditionally stable, and second-order accurate method with control over the dissipation of spurious high-frequency modes. The time step used in the simulations is small enough to satisfy the Courant–Friedrichs–Lewy condition.

3. Simulations of the free-field ultrasonic radiation

In this section, the acoustic response of a bulk piezoelectric element and the plate it is affixed to (if any) is examined in the time and frequency domains for the four configurations depicted in Fig. 2. The plates are made of steel with Lamé constants λ and μ equal to 145.95 and 75.19 GPa, respectively, and a mass density of 7850 kg m⁻³. The piezoelectric element is a PZT-5A ceramic with a mass density of 7750 kg m⁻³. The matrices needed in the linear electro-elastic constitutive relations of this piezoelectric material are given as,

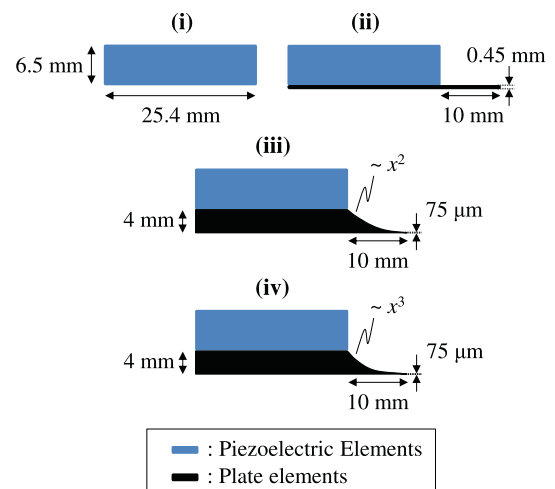


Fig. 2. The four configurations of ultrasonic transducers examined in this section.

$$\mathbf{c}^E = 10^9 \begin{bmatrix} 120.3 & 75.2 & 75.1 & 0 & 0 & 0 \\ 75.2 & 120.3 & 75.1 & 0 & 0 & 0 \\ 75.1 & 75.1 & 110.9 & 0 & 0 & 0 \\ 0 & 0 & 0 & 21.1 & 0 & 0 \\ 0 & 0 & 0 & 0 & 21.1 & 0 \\ 0 & 0 & 0 & 0 & 0 & 22.6 \end{bmatrix} \text{Pa} \quad (9)$$

$$\mathbf{e} = \begin{bmatrix} 0 & 0 & 0 & 0 & 12.3 & 0 \\ 0 & 0 & 0 & 12.3 & 0 & 0 \\ -5.4 & -5.4 & 15.8 & 0 & 0 & 0 \end{bmatrix} \text{C/m}^2 \quad (10)$$

$$\mathbf{\varepsilon}^S = 8.854 \times 10^{-12} \begin{bmatrix} 919.1 & 0 & 0 \\ 0 & 919.1 & 0 \\ 0 & 0 & 826.6 \end{bmatrix} \text{F/m} \quad (11)$$

The elastic solids are surrounded by air, with a mass density of 1.21 kg m^{-3} and a speed of sound of 343 m s^{-1} . In all simulations, the electric ground is imposed at the interface between the plate and the piezoelectric element while a pulse centered at 50 kHz with a peak amplitude of 50 V is imposed on its free horizontal face. This impulsive electrical loading, depicted in Fig. 3, induces the vibro-acoustic response of the system through the piezoelectric effect. The computational domains are discretized into triangular elements with a maximum element size of 0.5 mm. This size ensures convergence of the solution in the fluid domain (where the wavelength is the smallest) up to 137 kHz with five elements per wavelength. Simulations are carried out from 0 to 2 ms in steps of $1 \mu\text{s}$ (a total of 2001 time steps).

Fig. 4 shows snapshots of the acoustic pressures in the 2D fluid domains for the four transducer configurations depicted in Fig. 2. To characterize the spectral content of the far-field radiation, the magnitudes of the FFT of the acoustic pressures averaged along the exterior boundaries of the 2D fluid domains are also plotted in Fig. 5. It is also interesting to examine how the peak amplitudes of the acoustic pressures vary with time since they can relate to the performances of the TRMs used in Section 4: the operation of a TRM is a transient problem where energy is focused in time and space to achieve the highest possible amplitude. These quantities are plotted in the near and far fields in Fig. 6a and b, respectively. The peak amplitudes of the pressures are also plotted as a function of the thickness of a uniform plate in Fig. 7, to understand why a thickness of 0.45 mm was chosen in the numerical analysis. An animation of the near-field acoustic pressure radiated by the wedge of cubic profile due to the input voltage signal depicted in Fig. 3a is provided as a Supplementary movie file. A snapshot of this animation is shown in Fig. 8. The near-field radiation of this wedge was also computed using continuous-wave excitations at 43, 64, and 96 kHz, which correspond to some of the resonance frequencies observed in Fig. 5. The acoustic pressures at these frequencies are shown in Fig. 9.

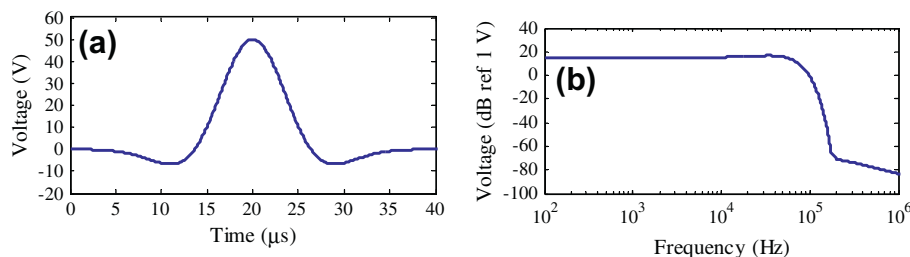


Fig. 3. Voltage signal imposed to the piezoelectric elements. (a) Time history. (b) Magnitude of the FFT.

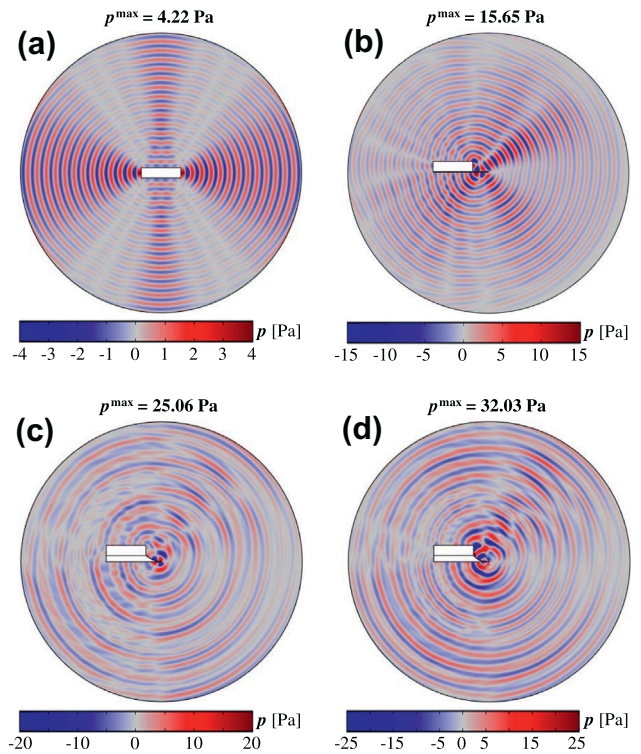


Fig. 4. Snapshots at time $t = 300 \mu\text{s}$ of the acoustic pressures in the 2D fluid domains for transducer configurations (a) 1, (b) 2, (c) 3, and (d) 4. The peak amplitudes of the acoustic pressures in the domains are indicated on top of the plots.

3.1. Isolated piezoelectric element

The radiation pattern of the isolated piezoelectric element depicted in Fig. 4a is characterized by beams of ultrasound emitted from the surfaces where fluid–structure interaction occurs. The aperture angle of these beams increases as the size of the radiating surface becomes small compared to the acoustic wavelength. For this reason, the aperture angle of the ultrasound beams radiated by the top and bottom surfaces is relatively small compared to that of the beams radiated by the side surfaces. The acoustic response of the isolated piezoelectric element is dominated by only one resonance, at 58 kHz, as shown in Fig. 5. Note that this transducer resonance corresponds to a radial type of motion: when the edges of the disc extend outward the middle of the disc compresses, and vice versa.

3.2. Piezoelectric element affixed to a thin plate of uniform thickness

When the piezoelectric element is affixed to the thin plate with a uniform thickness of 0.45 mm, the radiated wave field becomes

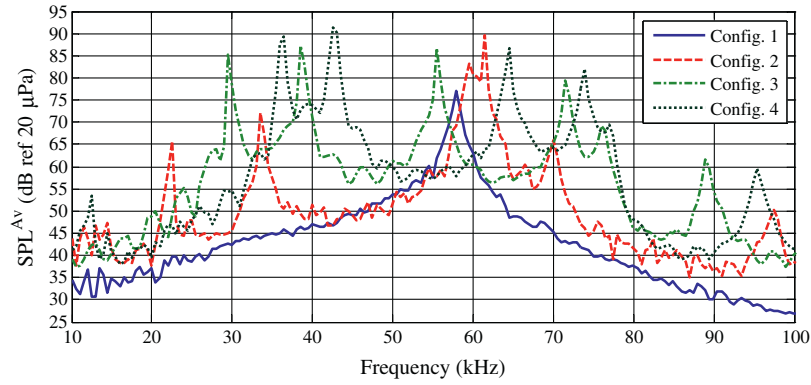


Fig. 5. Magnitudes of the FFT of the acoustic pressures averaged along the exterior boundary of the 2D fluid domains for the four transducer configurations.

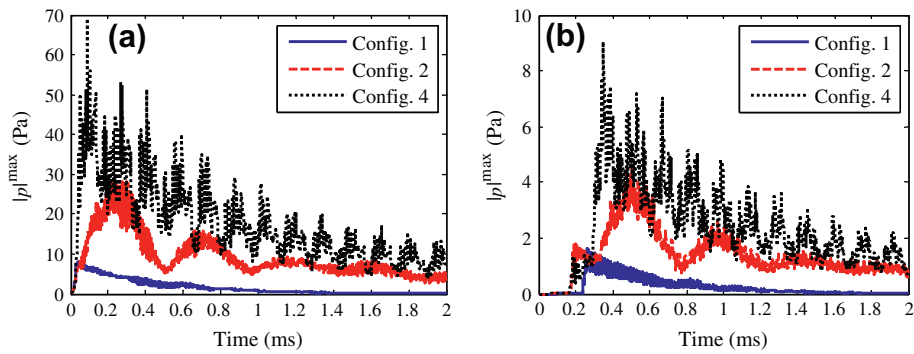


Fig. 6. Peak amplitudes of the acoustic pressures as a function of time for the transducer configurations 1, 2 and 4: (a) in the fluid domains: near field, and (b) along the boundaries of the fluid domains: far-field.

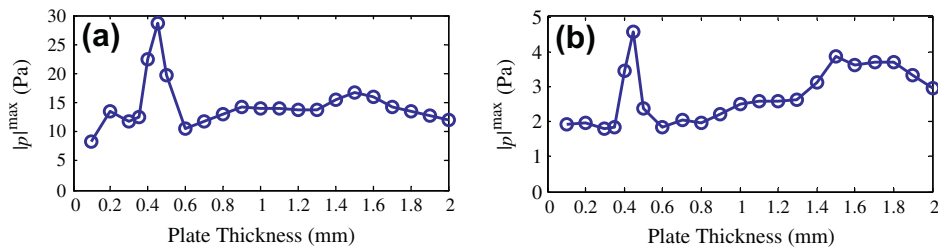


Fig. 7. Peak amplitude of the acoustic pressures as a function of the thickness of a uniform plate, (a) in the fluid domains: near field, and (b) along the boundaries of the fluid domains: far-field.

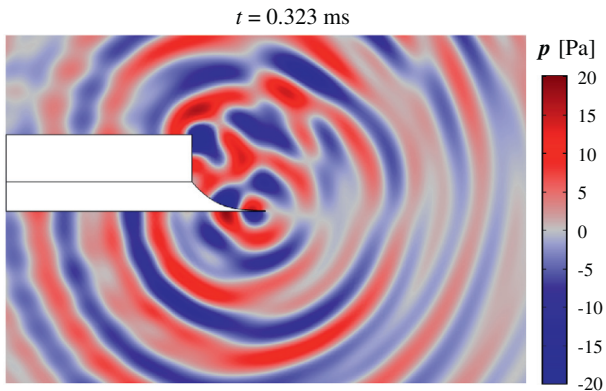


Fig. 8. Snapshot at time $t = 0.323$ ms of the acoustic pressure radiated by the wedge of cubic profile due to a pulse applied as input voltage to the Piezoelectric element. Animation provided as a [Supplementary file](#).

less directional (see Fig. 4b) while the peak amplitude of the acoustic pressure in the fluid domain is increased by $\times 3.6$ in the near-field and $\times 2.8$ in the far-field (see Fig. 6a and b), in comparison with the isolated piezoelectric element. As indicated in Fig. 5, the response of the transducer exhibits two dominant resonances near 60 kHz. The vibration motion of the free portion of the plate (not depicted here) resembles the third mode of a beam with one end free and the other end resting on elastic supports. A numerical eigenanalysis (not presented here) reveals that the natural frequency of the third bending mode for such a beam approaches 60 kHz. Therefore, around this frequency, the piezoelectric element enters in resonance with the plate, which results in an ultrasonic transducer with a significantly larger acoustic output but with mostly a narrow operating bandwidth. Indeed, the magnitude of the acoustic pressure at 61.5 kHz is at least 17 dB larger than that at any other resonance frequency (e.g. 22.5, 33.5, and 70 kHz). It is also important to mention that if the properties, dimensions, and/or boundary conditions of the plate change, so will its resonance frequencies. The plate may no longer enter in resonance with the

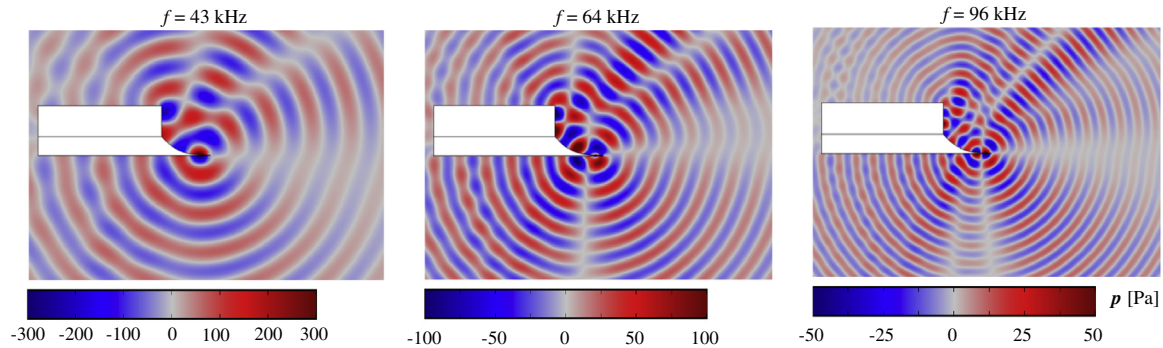


Fig. 9. Pressure radiated by the wedge of cubic profile in continuous-wave simulations at 43, 64, and 96 kHz: three of the resonance frequencies observed in Fig. 5. The peak-to-peak amplitude of the input voltage signal (continuous wave) is 30 V for all frequencies.

piezoelectric element and the acoustic radiation of the ultrasonic transducer may deteriorate. This is precisely what is observed in Fig. 7 as the plate thickness deviates from 0.45 mm.

3.3. Piezoelectric element affixed to thick plates with wedges of power-law profiles

The most significant changes in the acoustic response of the piezoelectric element are induced by the thick plates with wedges of power-law profiles. Fig. 4c and d shows that both profiles provide scattered fields with complex radiation patterns. The far-field radiation is dominated by six resonance frequencies, as shown in Fig. 5. The main difference with the thin plate of uniform thickness is the wider operating bandwidth of the transducer. For instance, the wedge of quadratic profile exhibits four resonances within an 8-dB magnitude range and over a 40-kHz frequency bandwidth. In terms of amplitude, the quadratic profile does not perform as well as the cubic profile. Note that no further improvements were found with a quartic profile (not presented here). Therefore, the analysis will be focused on the wedge of cubic profile. Fig. 6 indicates that the use of such a wedge may increase the peak amplitude of the acoustic pressure by $\times 8.5$ in the near field and $\times 5.5$ in the far field, relative to the radiation from the isolated transducer. It is also interesting to observe in Fig. 6 that the peak amplitude of the acoustic pressure radiated by the wedge does not vary smoothly

as a function of time, unlike that radiated by the isolated transducer, which is indicative of the multiple frequency components dominating the radiation. Figs. 4d, 8, and 9 suggest that most of the acoustic energy is radiated by portions of the wedge near the tip, thus providing a compact acoustic source. This result is consistent with the theoretical analysis outlined in Section 2.1. This compact source is rather complex and its characteristics depend on frequency. For instance, the near-field radiation resembles that from a dipole at 43 kHz but that from a quadrupole at 64 and 96 kHz. Therefore, at any instant, the wedge may radiate ultrasonic energy as a monopole, dipole, quadrupole, or any combination of these sources. This fact is clearly evidenced in Supplementary movie file. The complexity of the source partly explains the radiation patterns exhibited in Fig. 4d.

In a continuous-wave simulation, when the transducer with a wedge of cubic profile is driven at its resonance frequency of 43 kHz with a peak-to-peak amplitude of 30 V (see Fig. 9), the magnitude of the pressure reaches a maximum of 220 Pa (or a sound pressure level of 140.8 dB) at 12 mm from the wedge tip. As an indication, in Ref. [11] a piezoelectric MUT designed to operate near 41 kHz was made of a square-shaped membrane with a thickness of 7 μm and a side length of 2 mm. In a similar problem configuration (operating frequency, amplitude of the excitation, and distance from the source), the piezoelectric MUT generated a sound pressure level of 107 dB. Note that in a realistic 3D

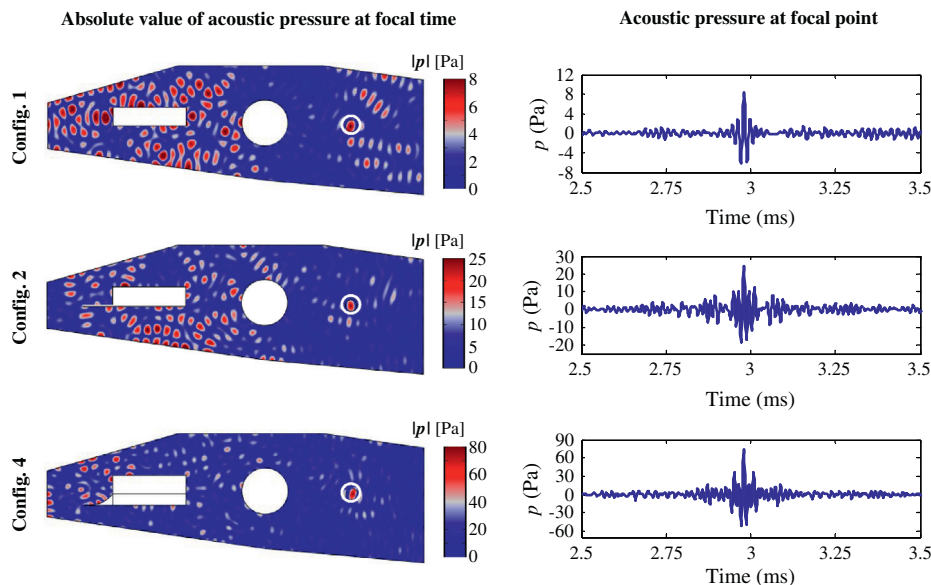


Fig. 10. Results from the numerical TR experiments for three transducer configurations. Left column: Snapshots at the focal time, $t = 2.98$ ms, of the absolute value of the acoustic pressures in the cavities. Right column: time histories of the acoustic pressures at the focal point.

experiment, the design proposed in this paper may not perform as well because of the imperfect bonding between the piezoelectric element and the plate but also because the far-field ultrasonic radiation due to a point-like source follows the cylindrical-spreading law in the 2D numerical simulations instead of the spherical-spreading law in a 3D problem. However, a wedge of cubic profile is still expected to enhance significantly the structural–acoustic coupling between bulk piezoelectric elements and the air. This remains to be quantified experimentally and will be the topic of some future work.

4. Simulations of time-reversal experiments

The analysis has been limited thus far in this paper to the free-field radiation from ultrasonic transducers. In this section, air-coupled TRMs are created by placing the transducers in cavities of arbitrary shapes with some perfectly reflecting surfaces. The transducer configurations 1, 2 and 4 depicted in Fig. 2 are considered in this analysis. Reciprocal TR is used to focus energy at a point in the cavity. In the forward-propagation step of the TR simulation, the pulse plotted in Fig. 3a is applied to the piezoelectric element and the acoustic response resulting at the desired focus point is recorded. Typically, in the back-propagation step, the recorded signal would be time reversed, normalized to have a given peak amplitude, and applied to the piezoelectric element. Here the signal is applied an inverse filter [30,31] instead of being time reversed, to improve the quality of the focal signal.

For each transducer configuration, the acoustic field inside the cavity at the focal time and the pressure waveform at the focal point are depicted in Fig. 10. The location where ultrasonic energy should be focused is indicated with a white circle. Animations of the pressures radiated by the transducers inside the cavity are provided as Supplementary movie files. For all three configurations, focus occurs at $t = 2.98$ s. With a bare piezoelectric element (configuration 1), the peak amplitude of the pressure at the focal point is 8.3 Pa. Even though ultrasonic energy is focused at the desired location, the acoustic field inside the cavity is contaminated by the presence of side lobes, whose amplitudes are often larger than that of the focus. The largest side-lobe amplitude is observed near a side of the piezoelectric element and is equal to 13.2 Pa (or $\times 1.6$ larger than the focus amplitude). When the piezoelectric element is affixed to a thin plate with a uniform thickness of 0.45 mm (configuration 2), the peak amplitude of the pressure at the focal point increases to 24.1 Pa, i.e. a gain of $\times 2.9$ compared to the isolated piezoelectric element. However, the number of side lobes with large amplitudes relative to the focus is still substantial. The most significant improvements in terms of increasing the amplitude of the focus and reducing that of the side lobes are observed with a wedge of cubic profile (configuration 4). The gain in pressure at the focus is $\times 9$ relative to the isolated piezoelectric element, with a peak amplitude of 74.6 Pa.

5. Conclusions

This paper examined the possibility of using wedges of power-law profile to enhance the ultrasonic radiation of bulk piezoelectric transducers in air. The analysis was supported by transient FE simulations of the ultrasonic radiation in 2D, both in the free field and in a reverberant environment. It was shown that when a piezoelectric element is affixed to a wedged plate, the elastic energy concentrates in the thinnest region of the wedge in the form of bending waves, resulting in a spatially compact source. Most of the acoustic energy is then generated near the wedge tip. The wedge extends the operating frequency bandwidth of the piezoelectric element and amplifies significantly the amplitude of its radiated pressure,

much more than a thin plate of uniform thickness would. In a simulated time-reversal experiment, the wedge increased the amplitude of the focus by an order of magnitude compared to a bare piezoelectric element. Meanwhile, the contribution of the spatial side lobes to the total ultrasonic field inside the reverberant cavity was reduced substantially, as a result of the extended frequency bandwidth.

The promising concept proposed in this paper needs to be validated and quantified experimentally. It could be integrated in the design of ultrasonic arrays of transducers, including TR mirrors, phased arrays, and parametric arrays. The analysis was limited to a relatively low frequency range (i.e. 10–100 kHz) to reduce the memory requirements of the numerical simulations. However, the device could be easily scaled to operate at higher frequencies.

Acknowledgements

We gratefully acknowledge the institutional support of the Los Alamos National Laboratory (LDRD program).

Appendix A. Supplementary material

Supplementary data associated with this article can be found, in the online version, at <http://dx.doi.org/10.1016/j.ultras.2014.02.017>.

References

- [1] J.D. Achenbach, Quantitative nondestructive evaluation, *Int. J. Solids Struct.* 37 (1–2) (2000) 13–27.
- [2] T.J. Ulrich, P.A. Johnson, R.A. Guyer, Interaction dynamics of elastic waves with a complex nonlinear scatterer through the use of a time reversal mirror, *Phys. Rev. Lett.* 98 (10) (2007) 104301.
- [3] M. Fink, G. Montaldo, M. Tanter, Time-reversal acoustics in biomedical engineering, *Annu. Rev. Biomed. Eng.* 5 (2003) 465–497.
- [4] G.F. Edelmann, H.C. Song, S. Kim, W.S. Hodgkiss, W.A. Kuperman, T. Akal, Underwater acoustic communications using time reversal, *IEEE J. Oceanic Eng.* 30 (4) (2005) 852–864.
- [5] T. Yano, M. Tone, A. Fukumoto, Range finding and surface characterization using high frequency air transducers, *IEEE Trans. Ultrason. Ferroelectr. Freq. Control* 34 (2) (1987) 232–236.
- [6] M.I. Haller, B.T. Khuri-Yakub, Micromachined 1–3 composites for ultrasonic air transducers, *Rev. Sci. Instrum.* 65 (6) (1994) 2095–2098.
- [7] H. Carr, C. Wykes, Diagnostic measurements in capacitive transducers, *Ultrasonics* 31 (1) (1993) 13–20.
- [8] I. Ladabaum, X. Jin, H.T. Soh, A. Atalar, B.T. Khuri-Yakub, Surface micromachined capacitive ultrasonic transducers, *IEEE Trans. Ultrason. Ferroelectr. Freq. Control* 45 (3) (1998) 678–690.
- [9] P. Murali, J. Baborowski, Micromachined ultrasonic transducers and acoustic sensors based on piezoelectric thin films, *J. Electroceram.* 12 (1–2) (2004) 101–108.
- [10] A. Hajati, D. Latev, D. Gardner, A. Hajati, D. Imai, M. Torrey, M. Schoeppler, Three-dimensional micro electromechanical system piezoelectric ultrasound transducer, *Appl. Phys. Lett.* 101 (25) (2012) 253101.
- [11] Z. Wang, W. Zhu, O.K. Tan, C. Chao, H. Zhu, J. Miao, Ultrasound radiating performances of piezoelectric micromachined ultrasonic transmitter, *Appl. Phys. Lett.* 86 (3) (2005) 033508.
- [12] B.W. Drinkwater, P.D. Wilcox, Ultrasonic arrays for non-destructive evaluation: a review, *NDT & E Int.* 39 (7) (2006) 525–541.
- [13] M. Fink, Time reversed acoustics, *Phys. Today* 50 (3) (1997) 34–40.
- [14] B.E. Anderson, C. Larmat, M.G. Griffa, T.J. Ulrich, P.A. Johnson, Time reversal, *Acoust. Today* 4 (1) (2008) 5–15.
- [15] A.M. Sutin, J.A. TenCate, P.A. Johnson, Single-channel time reversal in elastic solids, *J. Acoust. Soc. Am.* 116 (5) (2004) 2779–2784.
- [16] C. Draeger, M. Fink, One-channel time reversal of elastic waves in a chaotic 2D-silicon cavity, *Phys. Rev. Lett.* 79 (3) (1999) 407–410.
- [17] C. Draeger, M. Fink, One-channel time-reversal in chaotic cavities: theoretical limits, *J. Acoust. Soc. Am.* 105 (2) (1999) 611–617.
- [18] C. Draeger, J.-C. Aime, M. Fink, One-channel time reversal in chaotic cavities: experimental results, *J. Acoust. Soc. Am.* 105 (2) (1999) 618–625.
- [19] N. Etaix, M. Fink, R.K. Ing, Acoustic imaging device with one transducer, *J. Acoust. Soc. Am.* 131 (5) (2012) EL395–EL399.
- [20] N. Etaix, J. Dubois, M. Fink, R.K. Ing, Increasing the modal density in plates for mono-element focusing in air, *J. Acoust. Soc. Am.* 134 (2) (2013) 1049–1054.
- [21] P.-Y. Le Bas, T.J. Ulrich, B.E. Anderson, J.J. Esplin, A high amplitude, time reversal acoustic non-contact excitation (trance), *J. Acoust. Soc. Am.* 134 (1) (2013) EL52–EL56.

- [22] B. Arnal, M. Pernot, M. Fink, M. Tanter, Tunable time-reversal cavity for high-pressure ultrasonic pulses generation: a tradeoff between transmission and time compression, *Appl. Phys. Lett.* 101 (6) (2012) 064104.
- [23] V.V. Krylov, F.J.B.S. Tilman, Acoustic 'black holes' for flexural waves as effective vibration dampers, *J. Sound Vib.* 274 (3–5) (2004) 605–619.
- [24] V.V. Krylov, R.E.T.B. Winward, Experimental investigation of the acoustic black hole effect for flexural waves in tapered plates, *J. Sound Vib.* 300 (1–2) (2007) 43–49.
- [25] M.A. Mironov, Propagation of a flexural wave in a plate whose thickness decreases smoothly to zero in a finite interval, *Sov. Phys. Acoust.* 34 (3) (1988) 318–319.
- [26] V.V. Krylov, Localized acoustic modes of a quadratic solid wedge, *Mosc. Univ. Phys. Bull.* 45 (6) (1990) 65–69.
- [27] A. Leissa, *Vibration of Plates*, American Institute of Physics, New York, 1993.
- [28] COMSOL Users Guide, version 4.3 by COMSOL MULTIPHYSICS; web reference: <<http://www.comsol.com>> (Last viewed September 10, 2013).
- [29] J. Chung, G.M. Hulbert, A time integration algorithm for structural dynamics with improved numerical dissipation: the generalized- α method, *J. Appl. Mech.* 60 (2) (1993) 371–375.
- [30] M. Tanter, J.-F. Aubry, J. Gerber, J.-L. Thomas, M. Fink, Optimal focusing by spatio-temporal inverse filter. I. Basic principles, *J. Acoust. Soc. Am.* 110 (1) (2001) 37–47.
- [31] T.J. Ulrich, B.E. Anderson, P.-Y. Le Bas, C. Payan, J. Douma, R. Snieder, Improving time reversal focusing through deconvolution: 20 questions, *Proc. Meet. Acoust.* 16 (2012) 040515.